

A Parallel High-Order CENO Finite-Volume Scheme with AMR for Three-Dimensional Ideal MHD Flows

Lucie Freret, Clinton P.T. Groth, and Hans De Sterck

Abstract A highly-scalable and efficient parallel high-order finite-volume method with local solution-dependent adaptive mesh refinement (AMR) is described for the solution of steady plasma flows governed by the equations of ideal magnetohydrodynamics (MHD) on three-dimensional multi-block body-fitted hexahedral meshes, including cubed-sphere grids based on cubic-gnomonic projections. The approach combines a family of robust and accurate high-order central essentially non-oscillatory (CENO) spatial discretization schemes with a block-based anisotropic AMR scheme. The CENO scheme is a hybrid approach that avoids some of the complexities associated with essentially non-oscillatory (ENO) and weighted ENO schemes and is therefore well suited for application to meshes having irregular and unstructured topologies. The anisotropic AMR method uses a binary tree and hierarchical data structure to permit local refinement of the grid in preferred directions as directed by appropriately selected refinement criteria. Applications will be discussed for several steady MHD problems and the computational performance of the proposed high-order method for the efficient and accurate simulation of a range of plasma flows is demonstrated.

1 Introduction and Motivation

Physics-based space weather modeling [6, 7, 14] is a challenging problem that requires accurate numerical modeling for both disparate spatial and temporal scales. Accurate solutions can be achieved by using either high-order schemes or an adaptive mesh refinement (AMR) technique. A combination of both approaches would appear to be particularly desirable [15].

L. Freret (✉) • C.P.T. Groth

Institute for Aerospace Studies, University of Toronto, Toronto, ON, Canada M3H5T6
e-mail: lfreret@utias.utoronto.ca; groth@utias.utoronto.ca

H. De Sterck

School of Mathematical Sciences, Monash University, Melbourne, Australia
e-mail: hans.desterck@monash.edu

© Springer International Publishing AG 2017

M.L. Bittencourt et al. (eds.), *Spectral and High Order Methods for Partial Differential Equations ICOSAHOM 2016*, Lecture Notes in Computational Science and Engineering 119, DOI 10.1007/978-3-319-65870-4_24

343

The high-order central essentially non-oscillatory (CENO) finite-volume scheme from Ivan et al. [16, 18] uses a hybrid reconstruction approach based on a fixed central stencil. An unlimited high-order k -exact reconstruction is performed in the cells where the solution is well resolved while the scheme reverts to a low-order limited linear approach for cells with under-resolved/discontinuous solution content. Switching in the hybrid procedure is determined by a smoothness indicator. The CENO high-order scheme has been successfully applied to a broad range of flows on multi-block body-fitted meshes including non-viscous flows [18], viscous flows [16], large-eddy simulation (LES) of turbulent premixed flames [24] and magnetohydrodynamics (MHD) problems [18, 23]. The efficiency of the CENO scheme has also been assessed on cubed-sphere meshes [18] and extended to unstructured meshes for laminar viscous flows [5] and turbulent reactive flows [4].

Block-based AMR approaches [2, 3, 14, 21] are very attractive since they are naturally suitable for parallel implementation and lead to highly scalable methods while requiring an overall light data structure to compute the block connectivity. The multi-block AMR scheme considered here is based on the previous work by Gao and Groth [11] for reacting flows with isotropic refinement. This numerical scheme has also been applied to the solution of complex flow problems such as non-premixed laminar and turbulent flames [10, 12, 20] as well as turbulent multi-phase rocket core flows [22], MHD simulations [17, 18, 23], and micron-scale flows [13, 19]. The isotropic AMR scheme was originally extended to allow for anisotropic refinement by Williamschen and Groth [26] for non-viscous flows. More recently, Freret and Groth [9] reformulated the anisotropic AMR scheme using a non-uniform treatment of the cells (both interior and ghost or halo cells) within a given block. It directly makes use of the neighboring cells as the ghost cells, even those at different levels of refinement as found at grid resolution changes. The resulting anisotropic AMR multi-block scheme is better suited for high-order finite-volume schemes.

The focus of this study is the extension of the enhanced anisotropic AMR algorithm of Freret and Groth [9] for use in conjunction with the fourth-order CENO finite-volume scheme (the former permits the use of efficient high-order solution transfer operators) and the subsequent application of the combined method to the prediction of steady-state solutions of the ideal MHD equations. For this application, the solenoidal constraint on the magnetic field is controlled using the generalized Lagrange multiplier (GLM) proposed by Dedner et al. [8, 18, 23]. The ideal MHD equations and the GLM formulation are described in Sect. 2. In Sect. 3, a brief outline of the high-order CENO scheme is provided. The proposed anisotropic AMR block-based method is reviewed in Sect. 4 with the necessary extension for use with the high-order spatial discretization scheme. Finally, three-dimensional (3D) numerical results are presented in Sect. 5, including an accuracy demonstration of the high-order CENO reconstruction procedure for a known function and numerical results for two steady-state flow problems on cubed-sphere grids. Numerical results for both non-magnetized and magnetized flows are used to evaluate the grid convergence of the proposed fourth-order CENO scheme for uniformly and anisotropically refined meshes and compare the convergence behavior to that of the second-order limited method described by Ivan et al. [17].

The latter was originally developed for use with the isotropic AMR of Gao and Groth [11] and has been extended for the purpose of this study to non-uniform block-based anisotropic AMR.

2 Ideal Magnetohydrodynamics Equations

Solution of the hyperbolic system of ideal MHD equations is considered here using a high-order Godunov-type finite-volume scheme with a GLM formulation [8] which couples the divergence constraint, $\nabla \cdot \mathbf{B} = 0$, with the induction equation through the introduction of the potential, ψ . The system of conservation laws for which numerical solutions are sought may be expressed in weak conservation form as

$$\frac{\partial \mathbf{U}}{\partial t} + \nabla \cdot \mathbf{F} = \mathbf{S} + \mathbf{Q}, \quad (1)$$

where \mathbf{U} is the vector of conserved variables, \mathbf{F} is the solution flux dyad, and \mathbf{S} and \mathbf{Q} are volumetric source terms. The solution vector, \mathbf{U} , has the form

$$\mathbf{U} = [\rho, \rho \mathbf{V}, \mathbf{B}, \rho e, \psi]^T, \quad (2)$$

where ρ is the plasma density, \mathbf{V} the velocity field, \mathbf{B} the magnetic field, ρe is the total energy and ψ is the so-called generalized Lagrange multiplier variable associated with the GLM $\nabla \cdot \mathbf{B}$ treatment. The flux dyad, \mathbf{F} , is given by

$$\mathbf{F} = \begin{bmatrix} \rho \mathbf{V} \\ \rho \mathbf{V} \mathbf{V} + (p + \frac{\mathbf{B} \cdot \mathbf{B}}{2}) \mathbf{I} - \mathbf{B} \mathbf{B} \\ \mathbf{V} \mathbf{B} - \mathbf{B} \mathbf{V} + \psi \mathbf{I} \\ (\rho e + p + \frac{\mathbf{B} \cdot \mathbf{B}}{2}) \mathbf{V} - (\mathbf{V} \cdot \mathbf{B}) \mathbf{B} \\ c_h^2 \mathbf{B} \end{bmatrix}. \quad (3)$$

The specific total plasma energy is $e = p/(\rho(\gamma - 1)) + V^2/2 + B^2/(2\rho)$, where p is the molecular pressure, V is the magnitude of the fluid velocity, and B is the magnitude of the magnetic field. The numerical source term, \mathbf{S} , is due to the GLM-MHD formulation and has the form

$$\mathbf{S} = [0, \mathbf{0}, \mathbf{0}, 0, -\frac{c_h^2}{c_p^2} \psi]^T, \quad (4)$$

in which the coefficients c_p and c_h control the relative rates of dissipation and transport of ψ , as well as the corresponding advection speed of the $\nabla \cdot \mathbf{B}$ cleaning

mechanism, respectively. The ideal gas equation of state, $p = \rho RT$, is assumed, where T is the gas temperature and $R = 1/\gamma$ is the gas constant. For a polytropic gas (thermally and calorically perfect), the ratio of plasma specific heats, γ , is a constant, and the specific heats are given by $C_v = 1/(\gamma - 1)$ and $C_p = \gamma/(\gamma - 1)$. The source vector, \mathbf{Q} , appearing in Eq. (1) generally represents different volumetric sources arising from the physical modelling of various space plasma flows, such as gravitational forces.

2.1 Semi-Discrete Finite-Volume Formulation

The semi-discrete form of the preceding upwind finite-volume scheme applied to Eq. (1) for hexahedral computational cell (i, j, k) of a three-dimensional grid is

$$\frac{d\bar{\mathbf{U}}_{ijk}}{dt} = -\frac{1}{V_{ijk}} \sum_{f=1}^6 \sum_{m=1}^{N_g} (\tilde{\omega} \mathbf{F} \cdot \mathbf{n})_{i,j,k,f,m} + (\bar{\mathbf{S}})_{ijk} + (\bar{\mathbf{Q}})_{ijk} = (\bar{\mathbf{R}})_{ijk}(\bar{\mathbf{U}}), \quad (5)$$

where N_g is the number of Gauss quadrature points and \mathbf{n} is the local normal of the face f at each of the N_g Gauss quadrature points. The hexahedral cells are contained within logically Cartesian blocks that form a multi-block body-fitted mesh with general unstructured connectivity between blocks. The total number of Gauss integration points, N_g , at which the numerical flux is evaluated is chosen as the minimum required to preserve the targeted rate of convergence for solution accuracy. In this work, standard tensor-product quadrature consisting of four Gauss quadrature points are used for the cell faces, providing a fourth-order accurate spatial discretization. The latter is the target accuracy for the high-order scheme considered here.

The numerical fluxes, $\mathbf{F} \cdot \mathbf{n}$, at each Gauss quadrature point on each face of a cell (i, j, k) are determined from the solution of a Riemann problem. Given the left and right interface solution values, \mathbf{U}_l and \mathbf{U}_r , an upwind numerical flux is evaluated by solving a Riemann problem in the direction defined by the normal to the face. The values of \mathbf{U}_l and \mathbf{U}_r are determined by performing the CENO reconstruction as detailed in the next section. The contributions of the volumetric sources $\bar{\mathbf{S}}_{ijk}$, $\bar{\mathbf{Q}}_{ijk}$ are evaluated to fourth-order accuracy by again using a standard tensor-product Gauss quadrature with twenty-seven points for the volumetric integration. In the present computational studies, the Lax-Friedrichs approximate Riemann solver and fourth-order accurate Runge-Kutta explicit time-marching scheme have been used. Steady-state solutions are obtained using the latter by integrating the solution forward in time until a steady result is achieved.

3 High-Order CENO Finite-Volume Scheme

The hybrid CENO finite-volume method for conservation laws originally proposed by Ivan and Groth [16] is used to discretize the governing equations on a hexahedral computational grid. The hybrid CENO procedure uses the multidimensional unlimited k -exact reconstruction of Barth [1] in smooth regions and reverts to a limited piecewise-linear reconstruction algorithm in regions deemed as non-smooth or under-resolved by a solution smoothness indicator, thus providing monotone solutions near discontinuities.

In the present study, only smooth flows are considered reducing the CENO procedure to an unlimited fourth-order reconstruction. The K th-order Taylor series polynomial expansion of the spatial distribution of a scalar solution quantity, U_{ijk} , within a cell with index ijk about the cell-centroid $(x_{ijk}, y_{ijk}, z_{ijk})$ can be expressed as:

$$U_{ijk}(x, y, z) = \sum_{\substack{p_1=0 \\ (p_1+p_2+p_3 \leq K)}}^K \sum_{p_2=0}^K \sum_{p_3=0}^K (x - x_{ijk})^{p_1} (y - y_{ijk})^{p_2} (z - z_{ijk})^{p_3} D_{p_1 p_2 p_3}. \quad (6)$$

The coefficients, $D_{p_1 p_2 p_3}$, of the Taylor polynomials are referred to as the unknown derivatives and their number is equal to 20 for the target fourth-order accurate ($K = 3$ piecewise cubic) reconstruction. They are obtained by solving a constrained least-squares problem as detailed in Ivan et al. [16]. In order to obtain an exactly determined or overdetermined set of linear equations, a stencil including the two nearest rings of neighbours is used whatever is the mesh discretization size in the neighbouring cells. In particular, $5 \times 5 \times 5$ cells are used in a region with uniform resolution, and for regions with resolution changes or where the grid connectivity is irregular (such as at cubed-sphere sector edges), more or less numbers of cells may be used.

Both Householder QR factorization and singular value orthogonal decomposition (SVD) can be used to solve the weighted least-squares problem associated with the CENO reconstruction [16]. The latter is exploited here. The SVD approach permits the computation of a pseudo-inverse matrix after which the solution of the least-squares problem is then given by a simple matrix-vector product. The use of a single fixed stencil, the same for all dependent variables, allows the pseudo-inverse matrix to be stored and re-used in the reconstruction of all variables, thereby avoiding the repeated evaluation of the pseudo inverse. This was found to reduce significantly the computational costs of performing the CENO reconstruction without requiring substantial additional storage [16]. Additionally, there are conventionally issues with k -exact reconstruction related to conditioning and/or invertibility that generally increase with the order of the scheme as well as can be very dependent on mesh features, such as cell size, aspect ratio, and topology. However, a rather simple column-scaling procedure is applied here to the least-squares problem which significantly improves the conditioning, makes it virtually independent of the mesh, and affords robust and reliable solutions to the least-squares problem [16].

4 Parallel Anisotropic Block-Based AMR

A flexible block-based hierarchical binary tree data structure is used in conjunction with the spatial discretization procedure described in Sect. 2 to facilitate automatic solution-directed anisotropic mesh adaptation on body-fitted multi-block mesh. Figure 1 shows the resulting binary tree after several refinements of an initial mesh consisting of a single block. A binary tree is used rather than the usual octree used in isotropic methods, as the refinement decisions are made separately for each coordinate direction in the anisotropic AMR approach applied herein [9, 26].

The anisotropic AMR framework of Freret and Groth [9], based on extensions to the previous work by Williamschen and Groth [26], is well suited and readily allows the use of high-order spatial discretization by adopting a non-uniform representation of the cells within each block. An example of a non-uniform block obtained from a multi-block structure is shown in Fig. 2. In this treatment, the neighboring cells are used directly as the ghost cells, even those at different levels of refinement as found at grid resolution changes. This non-uniform treatment presents many advantages as outlined by Freret and Groth [9]. In particular, high-order

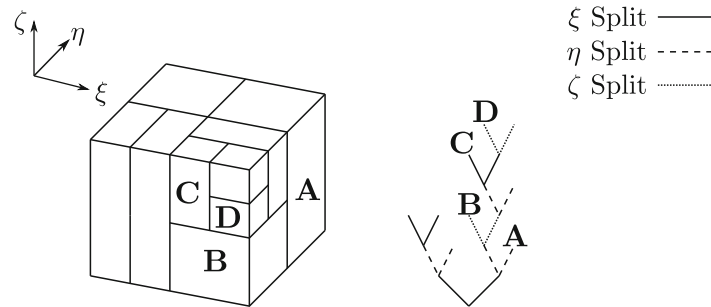


Fig. 1 3D binary tree and the corresponding blocks after several anisotropic refinements

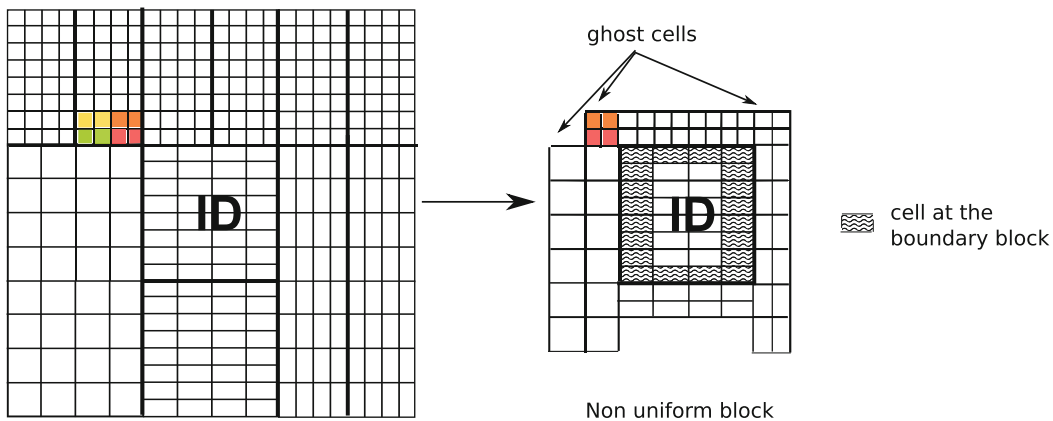


Fig. 2 Example of a non-uniform structured mesh block (*right*) obtained from a block-based anisotropic AMR grid mesh (*left*). This block is called non-uniform because its ghost cells may have different resolution from the interior cells

restriction and prolongation operators are not required to evaluate the solution within ghost cells.

Mesh adaptation is accomplished by refining and coarsening grid blocks. Each refinement produces new blocks called “children” from a “parent” block and the children can be refined further. This refinement process can be reversed in regions that are deemed over-resolved and two, four or eight children can coarsen or merge into a single parent block. In the present work we use a refinement criteria based on the gradient of a given quantity. This quantity can be a test function as in Sect. 5.1 or the fluid density as used in Sects. 5.2 and 5.3. The refinement criteria is a three-component vector such that the mesh can be refined in an anisotropic way.

A high-order accurate solution transfer from the coarse cell to the fine cells is required to distribute the average solution quantity among offspring with high-order accuracy. The high-order reconstruction polynomials of all solution variables on the coarse cell are readily integrated over the domain of each new fine cell having a volume, V_{fine} , and the resulting integrated average values of a solution quantity within the fine cells, \bar{u}_{fine} , is given by

$$\bar{u}_{fine} = \frac{1}{V_{fine}} \iiint_{V_{fine}} u_{coarse}(\mathbf{X}) dV = \frac{1}{V_{fine}} \sum_{m=1}^{N_g} \omega_m u_{coarse}(\mathbf{X}_m), \quad (7)$$

where the volume integral is computed exactly for the reconstruction polynomial with an appropriate-order tensor-product Gauss quadrature volumetric integration technique ($N_g = 27$ quadrature points are used for fourth-order spatial accuracy [16]). Here, ω_m and \mathbf{X}_m are the fine-cell Gauss weights and quadrature points.

5 Numerical Results

To validate the proposed fourth-order CENO finite-volume method for use in combination with the anisotropic AMR strategy outlined in Sect. 4, 3D numerical results are now considered, including a demonstration of the accuracy of the high-order CENO scheme for reconstruction of a known function and numerical predictions for steady-state flow problems on cubed-sphere grids. For the latter, numerical results for both non-magnetized and magnetized flows are used to evaluate the grid convergence of the CENO method when anisotropic AMR is applied. Additionally, the computational efficiency of the fourth-order CENO method is also compared to that of the second-order method described previously by Ivan et al. [17] and also extended herein for use in conjunction with the anisotropic AMR scheme.

5.1 Function Reconstruction on a Cubed-Sphere Grid

To demonstrate the accuracy of the CENO reconstruction applied in conjunction with anisotropic AMR, numerical results for the reconstruction of a smooth

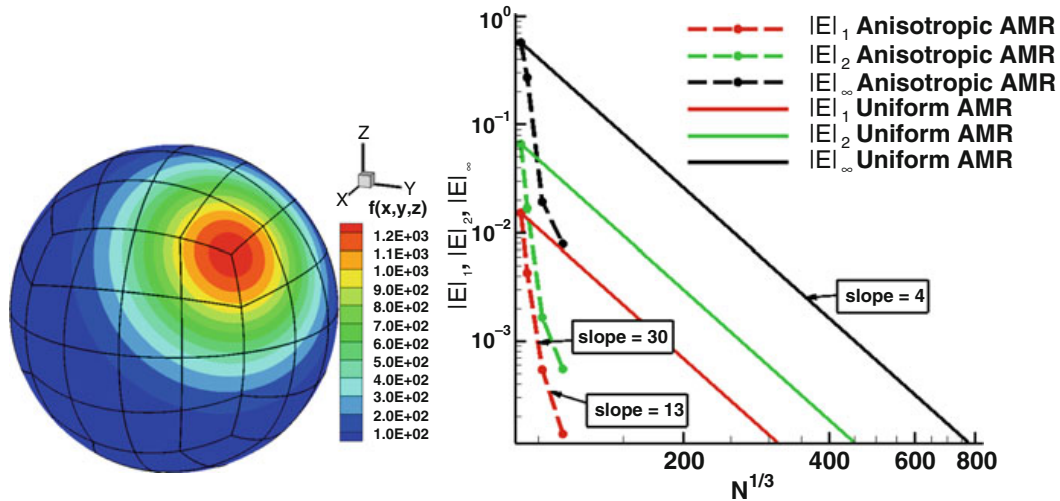


Fig. 3 (left) Contours of the test function f , (right) L_1 , L_2 , L_∞ error norms for the fourth-order CENO scheme with anisotropic AMR (dashed lines) compared to the error norms with fourth-order scheme with uniform refinements (solid lines)

continuous function are examined. This initial numerical test proceeds by first computing accurate cell averages for the function to be reconstructed and then using these cell averages to compute high-order polynomial reconstructions in the cells and finally computing the error between the original function and the polynomial reconstruction by high-accuracy numerical integration over each cell. The order of convergence of this error measures the order of accuracy of the CENO reconstruction. For the particularly case of interest, reconstruction of the function

$$f(x, y, z) = (1 - R + R^2)e^{x+y+z}, \quad (8)$$

is considered on the spherical computational domain defined by two concentric spheres with inner and outer radius $R_i = 1$ and $R_o = 3$, where R denotes the radius. As depicted in Fig. 3-left, this function exhibits a large smooth variation spanning several orders of magnitude that is oriented along the line connecting two diametrically-opposed cubed-sphere corners, where the function maximum and minimum occur. The computational meshes used in this grid convergence study range in size from 786,432 to 50,331,648 cells using from 96 to 6144 solution blocks. As shown in Fig. 3-right, the L_1 , L_2 , and L_∞ error norms obtained for the reconstruction procedure show that the CENO scheme achieves the theoretical fourth-order convergence accuracy when uniform refinements are applied (solid lines). The improved accuracy exhibited by the use of the anisotropic AMR translates into significant savings in terms of computational cell number for a targeted solution error. For example, to achieve $L_1 = 10^{-3}$ solution error, the fourth-order CENO method requires about 5,832,000 cells which is more than 5 times the mesh requirements when anisotropic AMR is applied. Moreover it is worth mentioning that the refinement criteria is based on the gradient of f defined

in Eq. (8) and user-defined thresholds for refinement and coarsening. Refinement strategies based on estimated solution error [25] are not applied here and therefore the mesh refinement does not guarantee a specific target solution accuracy. For this reason, the slopes of the error norms with AMR vary between 13 and 30, as shown in Fig. 3-right.

5.2 Steady Supersonic Outflow of Non-Magnetized Plasma

To assess the accuracy of the finite-volume scheme on cubed-sphere grids, numerical convergence studies for a spherically symmetric expanding supersonic non-magnetized plasma flow have been performed and are considered next. The accuracy of the fourth-order CENO scheme for a series of uniform and anisotropic refined AMR meshes was determined and is compared here to similar results obtained using the corresponding second-order scheme [17]. The computational domain of the steady supersonic outflow of interest is defined by inner and outer spheres of radius $R_i = 1$ and $R_o = 4$ respectively. For boundary data, the exact solution is imposed on the inner sphere: $\rho_i = 10$, $V_{r,i} = 4.5$, $\mathbf{V}_{\parallel,i=0}$ and $p_i = 26$. An outflow supersonic boundary condition is imposed at R_o . As described by Ivan et al. [17], the analytical solution of this flow problem can be obtained in spherical coordinates as the solution of the equation

$$C_3 - \frac{1}{r^2 V_r \left[(C_2 - V_r^2)^{\frac{1}{\gamma-1}} \right]} = 0, \tag{9}$$

where C_2 and C_3 are constants depending on the inflow conditions.

The L_1 , L_2 and L_∞ norms of the error in the predicted solution density obtained on a series of grids are given in Fig. 4. These convergence results show that

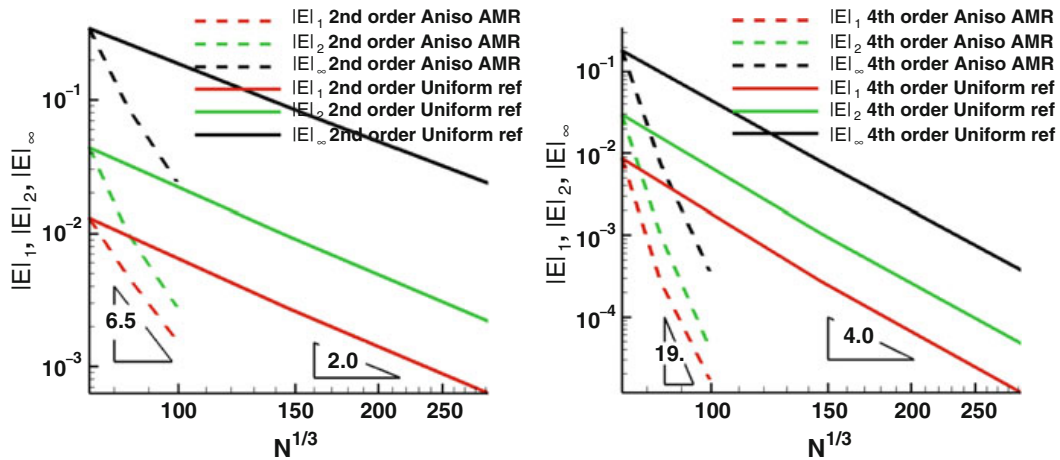


Fig. 4 L_1, L_2, L_∞ error norms for second-order (left) and fourth-order CENO schemes (right) with anisotropic AMR (dashed lines) compared to successive uniform refinements (solid lines)

the expected second-order (Fig. 4-left) and fourth-order (Fig. 4-right) theoretical accuracies are achieved in all error norms as the mesh is uniformly refined (solid lines). For anisotropic refinement of the mesh via the AMR strategy, the effective convergence rate approaches 6.5 for the second-order scheme and 19 for the CENO fourth-order scheme. As noted previously [9, 26], the solution varies only along the radial direction and the anisotropic AMR exploits this feature by refining only in the radial direction, thus avoiding the introduction of an unnecessary large number of computational cells. When the CENO scheme is used (Fig. 4-right), for an error target of $L_1 = 10^{-4}$, the memory requirement of the anisotropic AMR is only 12% of the memory requirement of the uniform refinements. For the second-order scheme (Fig. 4-left), for an error target $L_1 = 3 \times 10^{-3}$, the mesh saving of the anisotropic AMR strategy is around 73% compared to the uniform refinements. Finally, the mesh saving between second-order and fourth-order schemes with uniform refinements is about 90% for a target error of $L_1 = 10^{-3}$.

5.3 Steady Supersonic Outflow of Magnetized Plasma

As a final example, steady supersonic outflow of a magnetized plasma on a spherical domain is considered. The exact solution for this case is given by

$$\mathbf{U}(x, y, z) = \left[r^{-\frac{5}{2}}, \frac{x}{\sqrt{r}}, \frac{y}{\sqrt{r}}, \frac{z}{\sqrt{r}} + \kappa r^{\frac{5}{2}}, \frac{x}{r^3}, \frac{y}{r^3}, \frac{z}{r^3} + \kappa, r^{-\frac{5}{2}} \right]^T, \quad (10)$$

where $\kappa = 0.017$ is a perturbation parameter chosen such that the solution has significant latitudinal variation [17]. In Eq. (1), the source term \mathbf{Q} can be written as

$$\mathbf{Q} = \begin{bmatrix} 0 \\ \frac{1}{2}xr^{-\frac{5}{2}}(r^{-1} - 5r^{-2} - \kappa z) \\ \frac{1}{2}yr^{-\frac{5}{2}}(r^{-1} - 5r^{-2} - \kappa z) \\ \frac{1}{2}zr^{-\frac{5}{2}}(r^{-1} - 5r^{-2} - \kappa z) + \frac{5}{2}r^{-\frac{1}{2}}\kappa(1 + \kappa rz) + \kappa r^{-\frac{1}{2}} \\ 0 \\ \frac{1}{2}r^{-2} + \kappa z(3.5r^{-1} + 2\kappa z) + \frac{(\kappa r)^2}{2}(7 + 5\kappa rz) \end{bmatrix}.$$

The computational domain used for the outflowing plasma flow problem is defined by inner and outer spheres of radius $R_i = 2$ and $R_o = 3.5$. The inflow boundary conditions are specified at R_i based on the exact solution and outflow boundary conditions are applied at R_o .

The L_1 , L_2 and L_∞ norms of the error in the predicted solution density at cells centroids were obtained on a series of grids and are given in Fig. 5. As the mesh is uniformly refined, the theoretical fourth-order accuracy is achieved for the CENO scheme. When anisotropic AMR is applied the slopes of the L_1 , L_2 and L_∞ norms

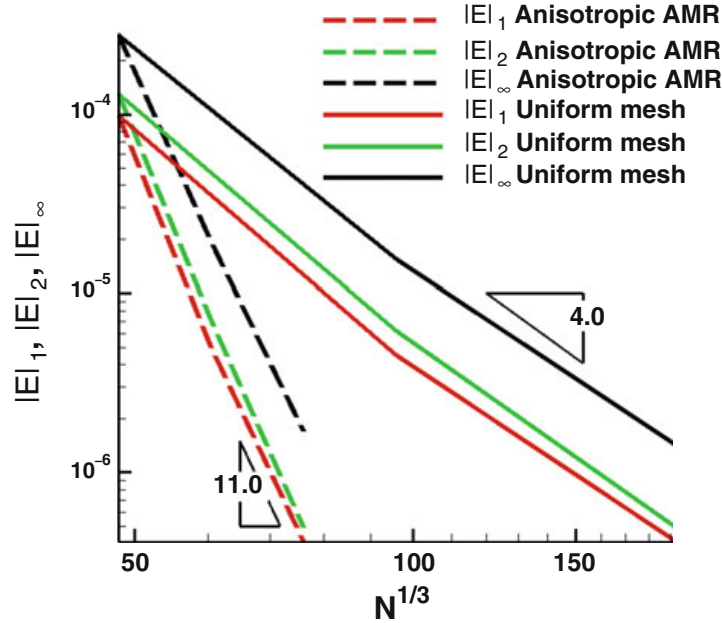


Fig. 5 L_1, L_2, L_∞ error norms of the solution density for the fourth-order CENO scheme with anisotropic AMR (*dashed lines*) compared to successive uniform refinements (*solid lines*)

are close to the value of 11. In terms of mesh size reduction, to achieve the error norm $L_1 = 10^{-6}$, the anisotropic AMR scheme uses only 9.2% of the number of cells of the uniform CENO scheme.

6 Conclusions

A fourth-order CENO finite-volume scheme has been extended for use with an efficient anisotropic block-based AMR method. High-order solutions on adapted anisotropic AMR grids have been obtained for three test problems on 3D cubed-sphere grids. The predicted results have been compared to those obtained using the high-order solution with uniform refinement as well as those of the associated second-order scheme, in order to assess the efficiency of the proposed approach. It is shown that high accurate solutions have been obtained with a reduced computational effort and significant reductions in mesh size. A natural future extension will be to consider the application to 3D unsteady MHD flows with both smooth solution content and shocks.

Acknowledgements This work was supported by the Canadian Space Agency and by the Natural Sciences and Engineering Research Council (NSERC) of Canada. In particular, the authors would like to acknowledge the financial support received from the Canadian Space Agency through the Geospace Observatory Canada program. Computational resources for performing all of the calculations reported herein were provided by the SciNet High Performance Computing

Consortium at the University of Toronto and Compute/Calcul Canada through funding from the Canada Foundation for Innovation (CFI) and the Province of Ontario, Canada.

References

1. T.J. Barth, Recent developments in high order k-exact reconstruction on unstructured meshes. Paper 93-0668, AIAA (1993)
2. J.B. Bell, M.J. Berger, J.S. Saltzman, M. Welcome, A three-dimensional adaptive mesh refinement for hyperbolic conservation laws. *SIAM J. Sci. Comput.* **15**(1), 127–138 (1994)
3. M.J. Berger, J. Olinger, Adaptive mesh refinement for hyperbolic partial differential equations. *J. Comput. Phys.* **53**, 484–512 (1984)
4. M.R.J. Charest, C.P.T. Groth, A high-order central ENO finite-volume scheme for three-dimensional turbulent reactive flows on unstructured mesh. Paper 2013–2567, AIAA (2013)
5. M.R.J. Charest, C.P.T. Groth, P.Q. Gauthier, A high-order central ENO finite-volume scheme for three-dimensional low-speed viscous flows on unstructured mesh. *Commun. Comput. Phys.* **17**(3), 615–656 (2015)
6. C.R. Clauer, T.I. Gombosi, D.L. De Zeeuw, A.J. Ridley, K.G. Powell, B. van Leer, Q.F. Stout, C.P.T. Groth, T.E. Holzer, High performance computer methods applied to predictive space weather simulations. *IEEE Trans. Plasma Sci.* **28**(6), 1931–1937 (2000)
7. D.L. De Zeeuw, T.I. Gombosi, C.P.T. Groth, K.G. Powell, Q.F. Stout, An adaptive MHD method for global space weather simulations. *IEEE Trans. Plasma Sci.* **28**(6), 1956–1965 (2000)
8. A. Dedner, F. Kemm, D. Kröner, C.D. Munz, T. Schnitzer, M. Wesenberg, Hyperbolic divergence cleaning for the MHD equations. *J. Comput. Phys.* **175**, 645–673 (2002)
9. L. Freret, C.P.T. Groth, Anisotropic non-uniform block-based adaptive mesh refinement for three-dimensional inviscid and viscous flows. Paper 2015–2613, AIAA (2015)
10. X. Gao, A parallel solution-adaptive method for turbulent non-premixed combustions flows, Ph.D. thesis, University of Toronto, 2008
11. X. Gao, C.P.T. Groth, A parallel solution-adaptive method for three-dimensional turbulent non-premixed combustions flows. *J. Comput. Phys.* **229**(5), 3250–3275 (2010)
12. X. Gao, S.A. Northrup, C.P.T. Groth, Parallel solution-adaptive method for two-dimensional non-premixed combustions flows. *Prog. Comput. Fluid Dyn.* **11**(2), 76–95 (2011)
13. C.P.T. Groth, J.G. McDonald, Towards physically-realizable and hyperbolic moment closures for kinetic theory. *Contin. Mech. Thermodyn.* **21**(6), 467–493 (2009)
14. C.P.T. Groth, D.L. De Zeeuw, T.I. Gombosi, K.G. Powell, Global three-dimensional MHD simulation of a space weather event: CME formation, interplanetary propagation, and interaction with the magnetosphere. *J. Geophys. Res.* **105**(A11), 25053–25078 (2000)
15. L. Ivan, Development of high-order CENO finite-volume schemes with block-based adaptive mesh refinement, Ph.D. thesis, University of Toronto, 2011
16. L. Ivan, C.P.T. Groth, High-order solution-adaptive central essentially non-oscillatory (CENO) method for viscous flows. *J. Comput. Phys.* **257**, 830–862 (2014)
17. L. Ivan, H. De Sterck, S.A. Northrup, C.P.T. Groth, Hyperbolic conservation laws on three-dimensional cubed-sphere grids: a parallel solution-adaptive simulation framework. *J. Comput. Phys.* **255**, 205–227 (2013)
18. L. Ivan, H. De Sterck, A. Susanto, C.P.T. Groth, High-order central ENO finite-volume scheme for hyperbolic conservation laws on three-dimensional cubed-sphere grids. *J. Comput. Phys.* **282**, 157–182 (2015)
19. J.G. McDonald, J.S. Sachdev, C.P.T. Groth, Application of Gaussian moment closure to micro-scale flows with moving and embedded boundaries. *AIAA J.* **51**(9), 1839–1857 (2014)
20. S.A. Northrup, C.P.T. Groth, Solution of laminar diffusion flames using a parallel adaptive mesh refinement algorithm. Paper 2005-0547, AIAA (2005)

21. J.J. Quirk, An adaptive grid algorithm for computational shock hydrodynamics, Ph.D. thesis, Cranfield Institute of Technology, 1991
22. J.S. Sachdev, C.P.T. Groth, J.J. Gottlieb, A parallel solution-adaptive scheme for predicting multi-phase core flows in solid propellant rocket motors. *Int. J. Comput. Fluid Dyn.* **19**(2), 159–177 (2005)
23. A. Susanto, L. Ivan, H.D. Sterck, C.P.T. Groth, High-order central ENO finite-volume scheme for ideal MHD. *J. Comput. Phys.* **250**, 141–164 (2013)
24. L. Tobaldini Neto, C.P.T. Groth, A high-order finite-volume scheme for large-eddy simulation of turbulent premixed flames. Paper 2014–1024, AIAA (2014)
25. D.A. Venditti, D.L. Darmofal, Anisotropic grid adaptation for functional outputs: application to two-dimensional viscous flows. *J. Comput. Phys.* **187**, 22–46 (2003)
26. M.J. Williamschen, C.P.T. Groth, Parallel anisotropic block-based adaptive mesh refinement algorithm for three-dimensional flows. Paper 2013–2442, AIAA (2013)